J Mater Sci (2006) 41:4382–4388
DOI 10.1007/s10853-006-0146-0

Structure determinations of double-wall carbon nanotubes grown by catalytic chemical vapor deposition

M. Gao · J. M. Zuo · R. Zhang · L. A. Nagahara

Received: 29 November 2005 / Accepted: 14 March 2006 / Published online: 28 June 2006

Abstract We report an application of nanoarea electron diffraction for structure determination of double-wall carbon nanotubes (DWNT) grown by catalytic chemical vapor deposition. The structures of 30 tubes were determined from experimental diffraction patterns. Among these tubes, the inner and outer wall structure of 18 tubes was precisely determined by comparison with kinematic electron diffraction simulations. For the structure of the DWNTs, our experiment revealed a mixture of semiconducting-metallic (S-M), S-S and M-M tubes. The spacing between the two walls ranges from 0.335 nm to 0.384 nm. Most DWNTs are incommensurate and chiral.

Introduction

Electron microscopy plays a critical role in nanomaterials research. While electron imaging gives direct information about the morphology and distribution of nanostructures, atomic resolution imaging and electron diffraction reveal atomic structure. With recent progresses in aberration-correctors, the resolution of electron microscopes and our ability to examine the details of atomic arrangements have further improved, especially for crystals. For nonperiodic structures and light atoms, the application of direct electron imaging is limited by the uncertainty of image interpretations and low signal-to-noise ratios in electron images. Electron diffraction is more suited for examining nonperiodic structures and for quantitative structure determination. Here, we illustrate the principle of electron diffraction structure determination of individual nanostructures using double-wall carbon nanotubes (DWNT) as an example.

A DWNT can be a combination of semiconducting-metallic (S-M), S-S, or M-M tubes. Whether a tube is semiconducting or metallic depends on the tube chiral vector [1]. Briefly, a carbon nanotube is a sheet of hexagonal covalently bonded carbon rolled up into a seamless tube. The structure of the tube is uniquely defined by its chiral vector $\vec{C} = n\vec{a} + m\vec{b}$, where the angle between $\vec{a}$ and $\vec{b}$ is 60°. The length and angle of $\vec{C}$ determine the tube diameter and chirality [2]. For a DWNT consisting of two concentric tubes, the structure is incommensurate if the outer and inner tubes have different chiral angles. The interaction between inner and outer tubes determines a variety of transport properties [3]. DWNTs have also attracted great interest as potential candidates for nanomachines due to the mechanical strength of the carbon nanotube and the weak Van der Waals interaction between the inner and outer walls [4]. For a DWNT, theory shows that the potential barrier between two chiral tubes can lead to different combinations for bolt-nut pair or discrete rotations [5].

While there are several techniques for characterizing single-wall carbon nanotubes [6–8], DWNT structure determination requires a penetrating probe, which has been

M. Gao · J. M. Zuo (✉)
Department of Materials Science and Engineering and Materials Research Laboratory, University of Illinois at Urbana, Champaign, IL 61801, USA
e-mail: jianzuo@uiuc.edu

R. Zhang · L. A. Nagahara
Physical Sciences Research Laboratories, Motorola Labs, 7700 South River Parkway, Tempe, AZ 85284, USA

M. Gao
Department of Electrical and Computer Engineering, Ohio State University, Columbus, OH 43210, USA

done only in a few cases using electron diffraction [9, 10]. As a result, our knowledge of DWNT structures is very limited. Here, we report on a systematic structure determination for 30 DWNTs. Previous difficulties in characterizing individual DWNTs were overcome by applying the new nanoarea electron diffraction (NED) technique that we developed based on a nanometer-sized parallel electron beam [7]. By recording electron diffraction patterns from individual DWNTs using this technique and by applying a new interpretation procedure, we show that most carbon nanotubes are chiral with preference for the chiral angles from 18° to 28°. About 1/3 of the tubes are metallic. From the chiral vectors of the 18 DWNTs determined unambiguously, we are able to measure the spacing between two tubes precisely and predict the electronic structure of each tube. We explain our results using growth energetics, which is also one of the major issues in carbon-nanotube research [11].

Only a single diffraction pattern is required for structure determination. The equatorial oscillations were used to measure the diameters of inner and outer walls and determine the tube structure. The ratios of layer line distances were used to measure chiral angles. This procedure has the advantage that the tube diameter measurement is separated from the structure determination of the tubes, in contrary to the case when high order layer lines are used [12].

Materials and methods

The carbon nanotubes studied here were grown by chemical vapor deposition (CVD). A catalyst (Fe:Mo:Al_2O_3) was prepared following the approach reported by Cassell et al. [13, 14]. The catalyst was either spun or sprayed onto the TEM grids then dried in a vacuum oven at 80 °C for 10 min before being loaded into the CVD reactor. CNT growth was performed in a hot-wall reactor fitted with a 3-in. horizontal quartz tube at 700–900 °C. Growth duration was 15 min with the reaction pressure at 10–100 Torr and the ratio of methane and hydrogen flow rate fixed at 60 sccm/min and 40 sccm/min, respectively. Both the number and structure of CNTs produced depends strongly on the growth temperature. In most cases, we observed a mixture of SWNTs and DWNTs. The percentage of DWNTs and the number of tubes (yield) increase with temperature. The yield also increases under higher reaction gas pressure. By varying the temperature and pressure, it is possible to grow CNTs of high density with dominantly SWNTs or DWNTs. For example, at 700 °C and 100 Torr of gas pressure, almost pure SWNTs were obtained, while at 800 °C, 10 Torr, more than 90% of the tubes were DWNTs.

The principle of NED has been described elsewhere [10, 15]. Briefly, with the condenser/objective setup shown in Fig. 1, a parallel illumination is formed by reducing the convergence angle of the condenser II crossover using the condenser mini-lens and placing the crossover at the focal plane of the objective prefield. For a condenser aperture of 10 μm in diameter, the probe diameter is ~50 nm with an overall magnification factor of 1/200 in a JEOL 2010F electron microscope. The size of the beam is much smaller than can be achieved using a selected area aperture. The diffraction pattern recorded in this mode is similar to SAED. For a crystal, the diffraction pattern consists of sharp diffraction spots. The major difference between NED and SAED is that the diffraction volume is defined directly by the electron probe in NED, which makes it more

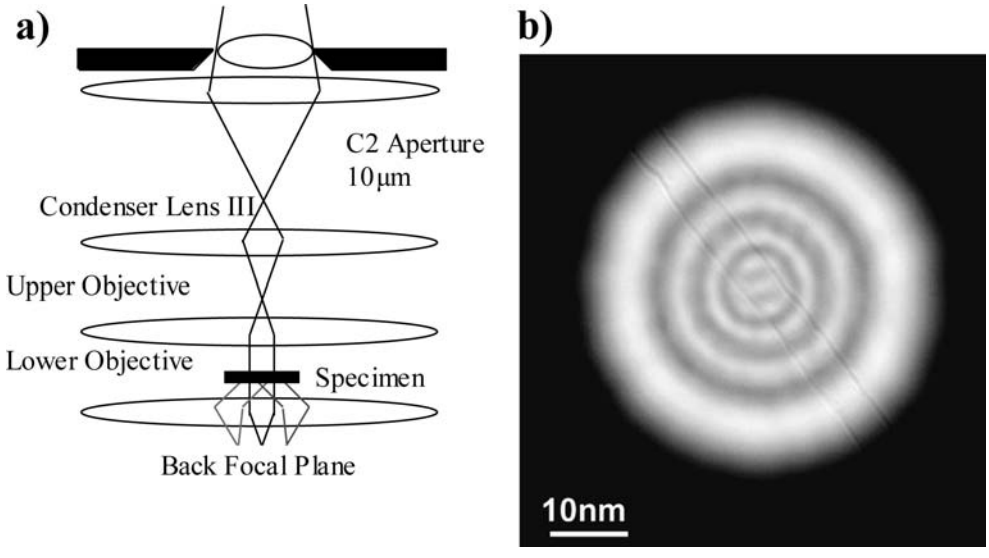

Fig. 1 Schematic diagram for NED (left); the electron probe formed with a 10-μm condenser aperture (right). This small probe is used to select a section of a carbon nanotube for electron diffraction. The tube is visible in the probe image. The intensity modulation comes from a large defocus used for forming the probe (see ref. 15)

efficient. Secondly, since all electrons illuminating the sample are recorded in the diffraction pattern, NED in a FEG microscope also provides higher beam intensity than SAED (the probe current density using a 10 μm condenser II aperture in JEOL 2010F is ~10^5 e/s-nm^2). The small probe size allows the selection of an individual nanostructure and a reduction of background intensities in recorded electron diffraction patterns from the surrounding materials.

The principle of DWNT structure determination by electron diffraction is shown in Fig. 2. To assign the chiral vectors of the inner wall and outer wall, we use the following procedure. First, we determine the two chiral angles using the first order diffraction lines, which form two hexagons (one of the two is shown in Fig. 2a). Following the method used for SWNT, the chiral angle is measured using

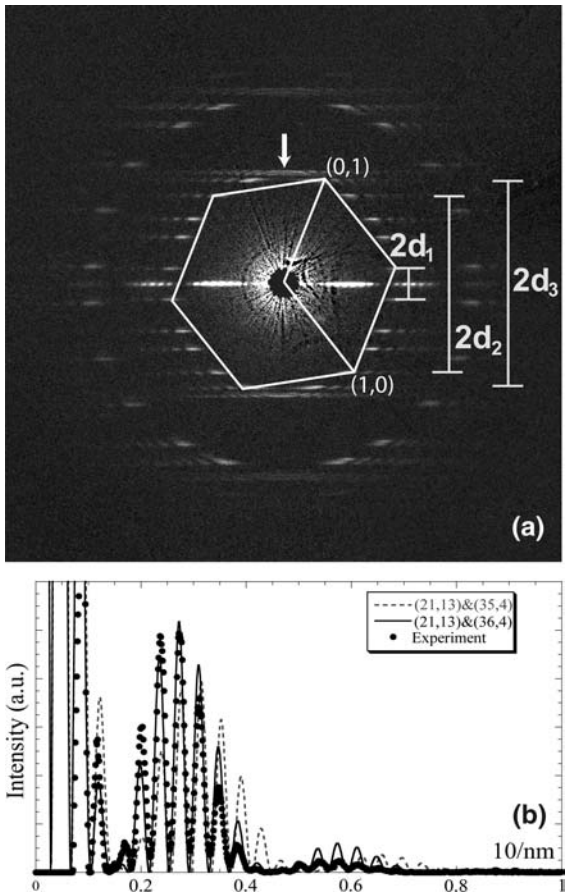

Fig. 2 The principle of DWNT structure determination (**a**) NED pattern from a DWNT, which was determined to be (36,4) and (21,13). The diffraction pattern consists of 4 hexagons, two each from the inner and outer tubes; the chiral angle of each tube was measured using the distance ratio method (see text). (**b**) The final tube structure was determined by matching the simulated and experimental equatorial oscillations. Two models are shown here, the large difference between the two shows the sensitivity of the equatorial oscillations to a small structural difference

$$\alpha = \mathrm{atan}\left(\frac{1}{\sqrt{3}} \cdot \frac{d_2 - d_1}{d_3}\right) = \mathrm{atan}\left(\frac{1}{\sqrt{3}} \cdot \frac{2d_2 - d_3}{d_3}\right) \qquad (1)$$

The chiral angle measurement using this technique is much more accurate than the direct measurement used previously [16]. For a straight tube, the accuracy is better than 0.2 ° (see ref. [7]). Secondly, we estimate the diameters of both walls from the equatorial oscillations. Based on the concentric DWNT model, the intensity along the equatorial line oscillates with a period of $\sim 1/\overline{D}$ ($\overline{D}$ is the averaged diameter of inner and outer tubes) within an oscillatory envelope of period of $1/\delta D$ (δD is the wall spacing). In the third step, we assign the chiral angles to inner and outer walls. This is achieved using the oscillations of first-order diffraction lines following the procedure described in [9]. The method is based on the order of Bessel functions, which described the intensity oscillations of the layer lines. For example, the intensity of the first-order diffraction line associated with the (1,1) reflection of the graphene sheet is described by the Bessel function of $n + m$ order [16]. Finally, we determine the chiral vectors of inner and outer tubes. To do this, we make a list of possible chiral vectors from the measured diameters and chiral angles with consideration of the measurement errors. The list of chiral vectors is limited to chiral angles between 0° and 30°. Two tubes of different handedness are not distinguished because of kinematic diffraction of the DWNTs. For each chiral vector, we match the experimental equatorial oscillation with the simulated one using the kinematical theory [7]. The final choice is selected from the best fit.

The DWNT giving the diffraction in Fig. 2a was determined to be (36,4) and (21,13) as follows. By measuring the distance ratios, we obtained two chiral angles of 5.2° and 22.3° with a difference of 17.1°. The average diameter and spacing are measured as 25.8 ± 0.4 Å and 3.27 ± 0.04 Å respectively. A list of possible structures is then generated for the inner tube. The tubes with diameter falling in the range (~2σ) of the measured diameter and chiral angle close to the two measured chiral angles (within ~2σ) are selected. The list is then used to simulate the first layer line for comparison with the experiment. The result is that the chiral angle of 22.3° belongs to the inner tube. Following this result, two lists of 3–4 structures for the inner and outer tubes respectively are selected using the same criteria as before. The combinations of inner and outer tubes are then used to simulate equatorial oscillations for comparison with the experiment. Figure 2b shows the profile of the experimental and simulated equatorial oscillations from two DWNTs of (21,13) and (36,4), (21,13) and (35,4). The large difference between the equatorial oscillations of the two models shows that the DWNT structure is uniquely determined by this procedure.

Simulation of carbon nanotube diffraction patterns

For the structure determination of a large diameter nanotube, we found that comparison between the experimental and simulated diffraction patterns is critical to distinguish the multiple choices for the tube structure given the uncertainty in experimentally measured chiral angles and tube diameters. To simulate the electron diffraction pattern of carbon nanotubes, we used the following procedure.

First, an atomic structure model is setup for each wall of the DWNT. The model is obtained by defining a rectangular supercell on the 2-D graphene sheet with the a'-axis as the chiral vector:

$$\begin{aligned} \overrightarrow{a}' &= \overrightarrow{C} = n\overrightarrow{a} + m\overrightarrow{b} \\ \overrightarrow{b}' &= j\overrightarrow{a} + k\overrightarrow{b} \end{aligned} \tag{2}$$

The b'-axis is selected as the shortest graphene lattice vector perpendicular to the a':

$$\overrightarrow{a}' \cdot \overrightarrow{b}' = 0 = nj + mk - (mj + nk)/2 \tag{3}$$

which leads to

$$\frac{j}{k} = \frac{n-2m}{2n-m}. \tag{4}$$

The values of j and k are selected as a pair of integers with no common factors other than 1. This new supercell thus defines the smallest repeating unit of the graphene sheet along the tube axis. In the second step, the atomic positions in the supercell are obtained by a transformation according to

$$\begin{pmatrix} x' \\ y' \end{pmatrix} = \frac{1}{nk - jm} \begin{pmatrix} k & -j \\ -m & n \end{pmatrix} \begin{pmatrix} x \\ y \end{pmatrix} \tag{5}$$

To construct the tube, the supercell defined in Eq. (2) is transformed so that the $\vec{b}'$-axis becomes the tube axis and the length, $|\vec{a}'|$, is the circumference of the tube. The atomic coordinates of the nanotube is obtained by taking

$$\begin{aligned} z'' &= y' \\ x'' &= r\cos\left(2\pi x'/\left|\overrightarrow{C}\right|\right) \\ y &= r\sin\left(2\pi x'/\left|\overrightarrow{C}\right|\right) \end{aligned} \tag{6}$$

In the second step, we use a direct summation of scattering from individual carbon atoms to calculate the structure factor of the tube:

$$U(k_x, k_y, k_z) = \sum_i f_i \exp\left[2\pi i\left(k_x x_i + k_y y_i + k_z z_i\right)\right] \tag{7}$$

The diffraction pattern itself is divided into pixels, the summation in Eq. (7) is carried over each pixel. For a carbon nanotube lying horizontally with the tube axis along the z direction and the electron beam along the y direction, k_y is taken as zero and k_x and k_z define the x and y direction of the diffraction pattern. We use Eq. (7) rather than the helical diffraction theory (outlined in Refs. [16–18] for simplicity and flexibility.

An example of a simulated nanotube diffraction pattern together with the structural model is shown in Fig. 3 for the (21,13) and (36,4) DWNT determined from the diffraction pattern in Fig. 2. Diffraction intensities were taken as proportional to $\left|U(k_x, k_y, k_z)\right|^2$. While the overall agreement between the experimental and simulated diffraction patterns is very good, there are some important differences. The most obvious difference is the intensity of the top diffraction line (indicated by the arrow). While the simulated diffraction pattern shows a clear gap, the experimental pattern has an arc-like feature, which indicates that the tube has a small curvature. Another noteworthy feature of the diffraction pattern is the interference between the two tubes. The two tubes are incommensurate, as a consequence, the electron diffraction from the two walls only interfere along the equatorial line.

Results and discussion

Figure 4a shows the structure of the 18 DWNTs determined using the previously described procedures. The tubes are labeled by a letter from 'a' to 'r'. The average diameter of the DWNTS ranges from 1.4 nm to 5.3 nm. The difference between the chiral angles of inner and outer walls ranges from 0.1° to 22.3°. Four DWNTs are very close to be commensurate with a chiral angle difference smaller than 0.3°. These tubes are marked by 'k', 'l', 'm' and 'r' in Fig. 3a. One of these tubes ('m'), (34,8) and (42,10), is nearly commensurate with a chiral angle difference of 0.1°.

The electronic structure of a perfect cylindrical SWNT can be predicted based on its chiral vector (n,m) [2]. If n-m can be evenly divided by 3 (defined with $\measuredangle(\vec{a}, \vec{b}) = 60°$), the SWNT is metallic or semi-metallic with a very small band gap. Otherwise, the SWNT is semiconducting [1]. Using this rule, we predicted the electronic structure of each tube based on the experimentally determined tube structure [19]. The results are shown in Fig. 4a. Among the observed DWNTs, there are 8 S-S, 7 M-S and 3 M-M tubes. For the inner tubes, 7 are metallic and 11 are semiconducting. For the outer tubes, 6 are metallic and 12 are semiconducting. The ratio of metallic and semiconducting tubes is the same as the 1:2 ratio predicted based on

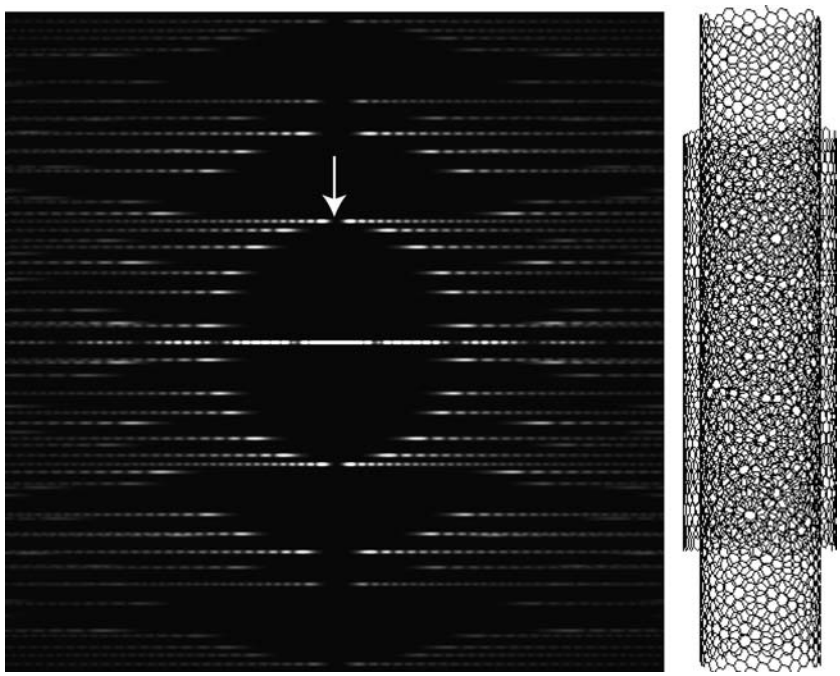

Fig. 3 Simulated electron diffraction pattern for the nanotube structure determined from Fig. 2 (left), and the atomic structure model (right)

a random selection and there is no preferred conductivity for either the inner or outer walls of the DWNTs.

The distribution of wall spacing is shown in Fig. 4b. The wall spacing ranged from 0.331 nm to 0.378 nm with a mean value of 0.361 nm. Its dependence on both the tube diameter and the difference between two chiral angles is random. The distribution of wall spacing shown in Fig. 4b can be qualitatively explained by the weak van der Waals interaction between inner and outer walls. However, the calculation results of Saito et al. [5] show a relatively flat minimum from 0.33 nm to 0.35 nm with the lowest energy at 0.34 nm wall spacing, which is very close to the ~0.344 nm interlayer distance in turbostratic graphite with uncorrelated graphene layers (single-crystal graphite has a layer spacing of 0.3354 nm). It is important to note that the increased layer spacing in turbostratic graphite comes from stacking disorder (deviation from the perfect AB stacking), which is very different from an incommensuate DWNT, which has no fixed registry of carbon atoms between the inner and outer tubes. This is expected to result in a larger interlayer spacing.

The chiral angle distribution of 30 DWNTs (60 walls) is summarized in Fig. 5 [20]. The chiral-angle distribution is not random as expected from the geometry of a graphene sheet. There is a clear preference for chiral angles from 18° to 28° with 29 out of 60 walls falling into this range. There are only few pure zig-zag and armchair walls. The lack of preference for armchair tubes means that most metallic tubes are the small-gap type.

The preferred chiral growth in CVD carbon nanotubes can not be explained based on the tube energetics alone, e.g. the lack of armchair tubes is contrary to the argument that the armchair tube is the energetically favored nanotube structure [21]. In low-temperature CVD, carbon nanotubes grow by protruding from the catalyst particle at the tube–solid interface, where carbon atoms or molecules attach to the tube. The abundance of chiral tubes of near armchair configuration suggests a favored growth by hexagon addition with carbon dimers at the interface as illustrated in Fig. 6. For CNTs, the fraction of sites for dimer attachment increases from 0% to 100% as α increase from 0° to 30°. This is at the expense of the interface energy, which also

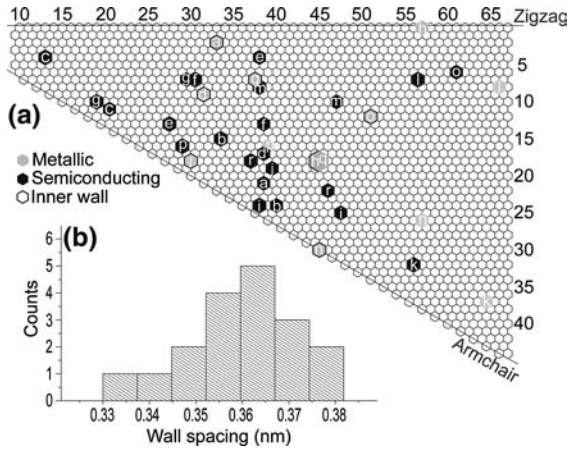

Fig. 4 (**a**) Statistic results from the 18 DWNTs, which were marked as 'a'–'r' on the graphite lattice. Lightly and heavily filled hexagons represent metallic (including semi-metallic) and semiconducting cells respectively. The hexagons with marked edges indicate inner walls. (**b**) Distribution of the wall spacings

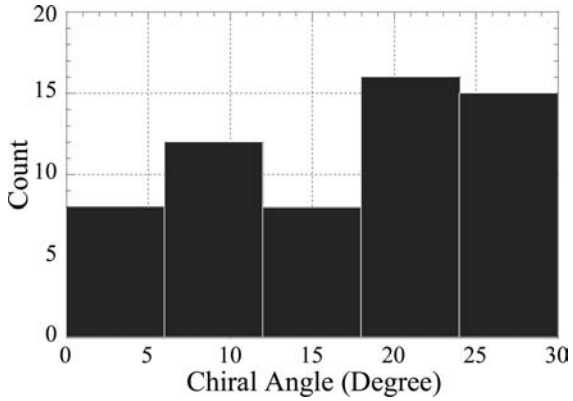

Fig. 5 Chiral angle distribution for 30 DWNTs, which contains 60 tubes in total. Among these tubes, there were only 2 zig-zag tubes and one armchair tube. The remaining are chiral

increases (a zig-zag tube has 0.406 carbon–metal bonds per Å compared to 0.515 for an armchair tube). The lack of armchair tubes can be explained based on growth energetics; in the classical growth theory the interface process controlled growth rate is proportional to $|\Delta G| \exp[-q/kT]/kT$, where q is the interfacial energy barrier and $|\Delta G|$ is the driving force. The energy barrier q includes a bond-breaking term for carbon–metal bonds at the nanotube and catalyst interface. For a pure zig-zag or armchair tube, all bonds have to be broken in order to grow an additional layer, while for a chiral tube, only a few bonds need to be broken (see Fig. 6). Thus, we propose that carbon nanotubes grow by preferential attachment to steps that come with a chiral tube, and the growth is very much like the Frank's growth model for real crystals where steps formed by dislocations flow by preferential attachment.

Conclusions

In conclusion, NED was used to determine the structure of individual DWNTs grown by low-temperature catalytic CVD. A nanotube structure determination procedure was developed based on kinematic diffraction and comparison with simulation. Among the observed DWNTs, there is a

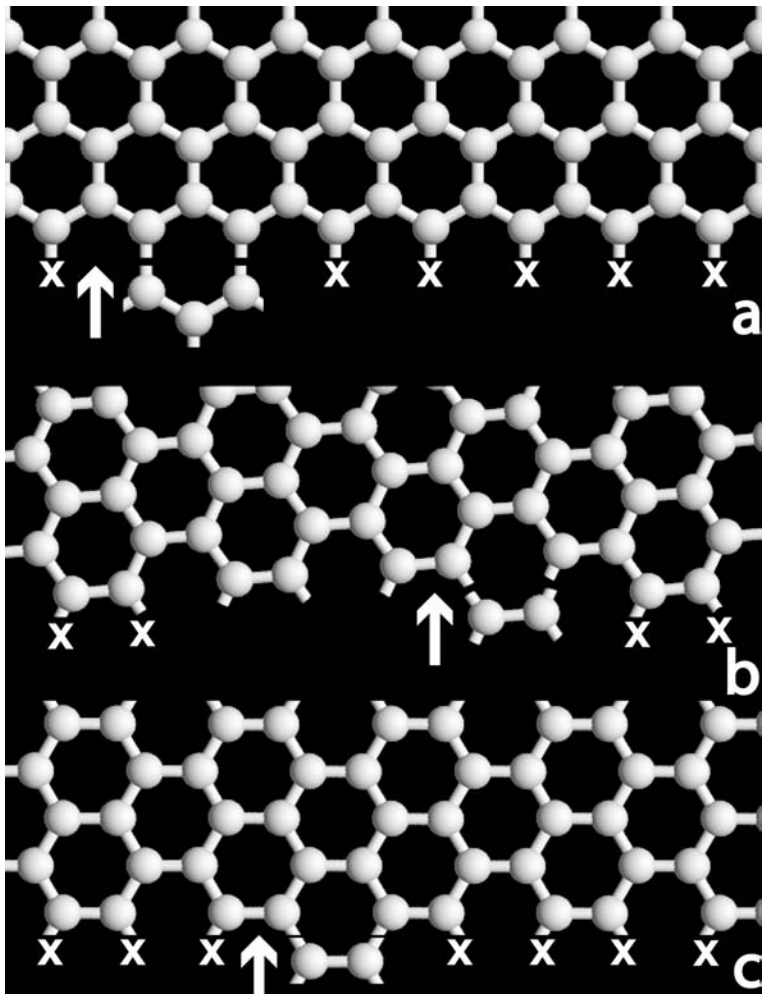

Fig. 6 Hexagon growth of zig-zag (left), chiral (α = 25 °) (middle) and armchair carbon nanotubes with horizontal tube direction (right). Both the chiral and armchair nanotubes grow by addition of carbon dimers, while the zig-zag tubes require a combination of carbon trimers, dimers and monomers. The X marks the carbon–metal bond at the nanotube and catalyst interface. The stepped tube–metal interface of a chiral tube requires few bond breakings and provides favored attachment sites as shown by the arrow

mixture of S-S, M-S and M-S tubes. We found no preferred conductivity for the inner and outer walls of DWNTs. The structure of DWNTs is non-uniform; tubes close to the armchair configuration are favored and the average wall spacing is 0.36 nm. We explained these results by proposing a step growth model for carbon nanotubes.

Acknowledgements Work on electron microscopy characterization is supported by DOE DEFG02-01ER45923 and DEFG02-91ER45439 and uses the TEM facility of Center for Microanalysis of Materials at FS-MRL. M.G. thanks Dr. M. Kociak for discussions.

References

1. Theory predicts for a metallic tube if (n-m) = 3l (l: an integer) or a semiconducting tube for n-$m \neq 3l$; see Mintmire JW, Dunlap BI, White CT (1992) Phys Rev Lett 68:631 and Saito R, Fujita M, Dresselhaus G, Dresselhaus MS (1992) Appl Phys Lett 60: 2204
2. Saito R, Dresselhaus G, Dresselhaus MS (1998) Physical properties of carbon nanotubes. Imperial College Press, London
3. Uryu S (2004) Phys Rev B 69:075402
4. Cumings J, Zettl A (2000) Science 289:602
5. Saito R, Matsuo R, Kimura T, Dresselhaus G, Dresselhaus MS (2001) Chem Phys. Lett 348:187
6. Jorio A, Saito R, Hafner JH, Lieber CM, Hunter M, Mcclure T, Dresselhaus G, Dresselhaus MS (2001) Phys Rev Lett 86:1118; Bachilo SM, Strano MS, Kittrell C, Hauge RH, Smalley RE, Weisman RB (2002) Science 298:2361
7. Gao M, Zuo JM, Twesten RD, Petrov I, Nagahara LA, Zhang R (2003) Appl Phys Lett 82:2703
8. Qin L-C, Iijima S, Kataura H, Maniwa Y, Suzuki S, Achiba Y (1997) Chem Phys Lett 268:101
9. Kociak M, Hirahara K, Suenaga K, Iijima S (2003) Euro Phys J B 32:457
10. Zuo JM, Vartanyants I, Gao M, Zhang R, Nagahara LA (2003) Science 300:1419
11. Dresselhaus MS, Dai HJ (2004) Mater Res Soc Bull 29:237
12. Liu Z, Zhang Q, Qin LC (2005) Appl Phys Lett 86:191903
13. Cassell AM, Raymakers JA, Kong J, Dai HJ (1999) Phys Chem B 103:6484
14. Zhang R, Tsui RK, Tresek J, Rawlett AM, Amlani I, Hopson T, Fejes P (2003) J Phys Chem B 107:3137
15. Zuo JM, Gao M, Tao J, Li BQ, Twesten R, Petrov I (2004) Microsc Res Techniq 64:347
16. Qin LC (2001) In: Zhang XF, Zhang Z (eds) Progress in transmission electron microscopy, vol 2. Springer-Verlag, Berlin
17. Lambin P, Lucas AA (1997) Phys Rev B 56:3571
18. Amelinckx S, Lucas A, Lambin P (1999) Rep Prog Phys 62:1471
19. The experimentally determined structure is the best model of ideal cylindrical tubes that fits the experimental diffraction pattern
20. We selected 30 DWNTs randomly. Among these, 12 DWNTs are slightly curved, the diffraction patterns of these tubes were not sufficiently clear to determine the chiral vectors unambiguously. For these tubes, the mean diameter and chiral angles were measured at resolutions of 3% and 0.5° respectively
21. Thess A, Lee R, Nikolaev P, Dai H, Petit P, Robert J, Xu C, Lee YH, Kim SG, Rinzler AG, Colbert DT, Scuseria GE, Tomanek D, Fischer JE, Smalley RE (1996) Science 273:483